A single-beam NIR laser triggered full-color upconversion tuning of Er/Tm: $CsYb_2F_7$@glass photothermal nanocomposite for optical security

Jiwen Zhu [a,b], Shaoxiong Wang [a,*], Zezhong Yang [a], Shengxiang Liao [a], Jidong Lin [a], Hurong Yao [a,*], Feng Huang [a, c, d], Yuanhui Zheng [b,e], Daqin Chen [a,b,c,d *]

[a] College of Physics and Energy, Fujian Normal University, Fujian Provincial Key Laboratory of Quantum Manipulation and New Energy Materials, Fuzhou, 350117, China

[b] Fujian Science & Technology Innovation Laboratory for Optoelectronic Information, Fuzhou, 350116, China

[c] Fujian Provincial Collaborative Innovation Center for Advanced High-Field Superconducting Materials and Engineering, Fuzhou, 350117, China

[d] Fujian Provincial Engineering Technology Research Center of Solar Energy Conversion and Energy Storage, Fuzhou, 350117, China

[e] College of Chemistry, Fuzhou University, Fuzhou, 350116, China

Table S1 Color coordinates for laser power dependent UC luminescence yielded from the Tm/Er: $CsYb_2F_7$@glass under the irradiation of 980 nm laser.

Laser power density (W/cm^2)	0.25%Tm-0.25%Er		0.25%Tm-0. 5%Er		0.25%Tm-0.75%Er		0.25%Tm-1%Er	
	CIE x	CIE y	CIE x	CIE y	CIE x	CIE y	CIE x	CIE y
33	0.2314	0.1686	0.3435	0.2703	0.3908	0.3107	0.4121	0.3411
51	0.2872	0.2463	0.3548	0.3216	0.3955	0.3443	0.4221	0.3707
70	0.3354	0.3029	0.3611	0.3862	0.3992	0.3919	0.4258	0.4091
89	0.339	0.3509	0.3512	0.4525	0.3884	0.4405	0.409	0.463
108	0.3276	0.4253	0.3164	0.5373	0.3549	0.5064	0.3598	0.5337
126	0.3041	0.4927	0.291	0.5874	0.3228	0.5549	0.3074	0.5934
146	0.2916	0.5337	0.2954	0.5913	0.3021	0.5891	0.282	0.6305

Table S2 Color coordinates for laser power dependent UC luminescence yielded from the Er/Tm: $CsYb_2F_7$ NCs@glass after covering with a cut-off optical filter above 495 nm pass-through.

Laser power density (W/cm^2)	CIE x	CIE y
33	0.5922	0.3909
51	0.5362	0.4408
70	0.5006	0.4722
89	0.4766	0.4944
108	0.4437	0.5244
126	0.3975	0.5663
146	0.3626	0.5983

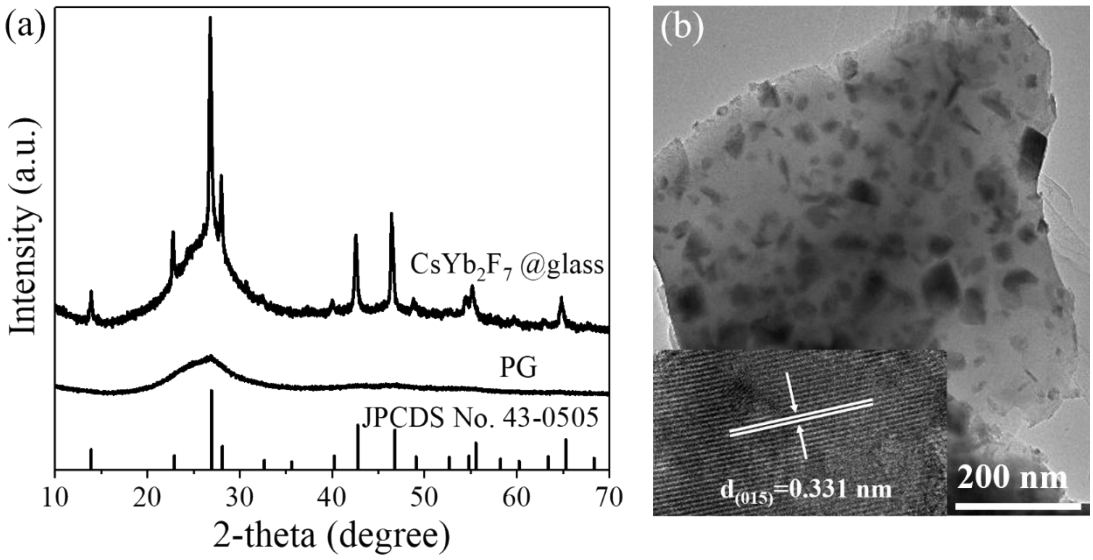

Fig. S1. (a) XRD patterns of PG and $CsYb_2F_7$ NCs@glass prepared by heating PG at 900 °C for 2 h. (b) TEM image of a typical $CsYb_2F_7$ NCs@glass sample, inset is the corresponding HRTEM image.

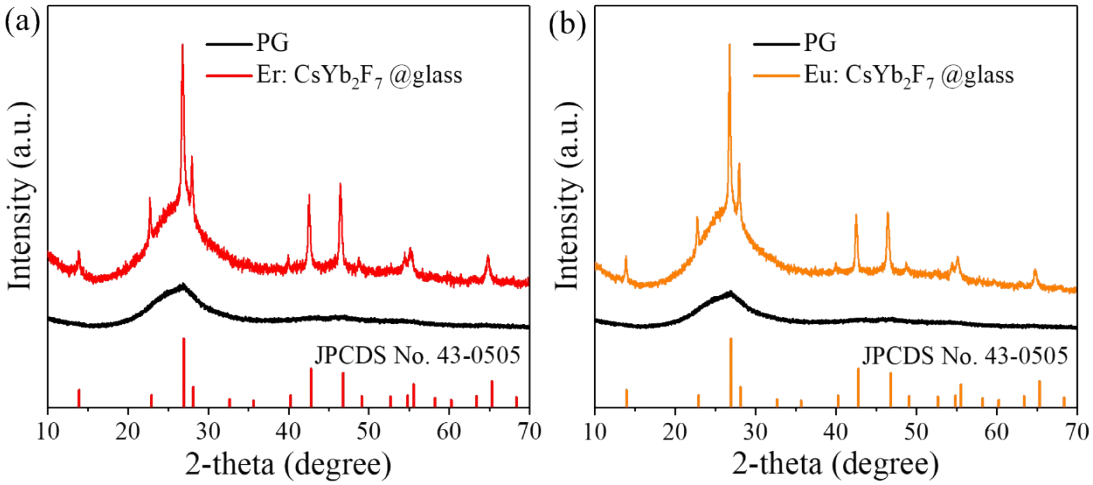

Fig. S2. XRD patterns of (a) Er and (b) Eu doped PG and $CsYb_2F_7$ NCs@glass samples prepared by annealing PGs at 900 °C for 2 h.

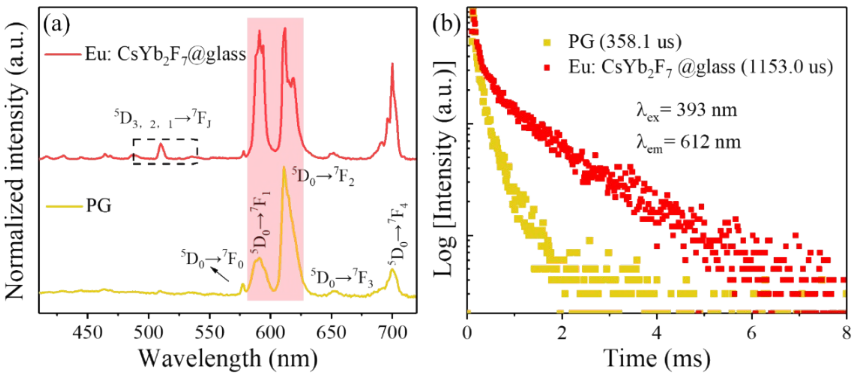

Fig. S3. (a) PL spectra (λ_{ex} = 393 nm) of Eu-doped PG and $CsYb_2F_7$ NCs@glass and (b) the corresponding decay curves by monitoring Eu^{3+}: $^5D_0 \rightarrow {}^7F_2$ transition (612 nm).

The present NCs@glass composites were prepared by heating precursor glasses. Therefore, after glass crystallization, the crystal-field environment around Eu^{3+} is altered from amorphous aluminosilicate glass with large phonon energy and low symmetry into $CsYb_2F_7$ crystal lattice with low phonon energy and high symmetry. Consequently, the decrease of the intensity ratio between $^5D_0 \rightarrow {}^7F_2$ electric-dipole transition and $^5D_0 \rightarrow {}^7F_1$ magnetic-dipole one is mainly ascribed to the change of the crystal-field environment around Eu^{3+} from amorphous aluminosilicate glass into crystal lattice.

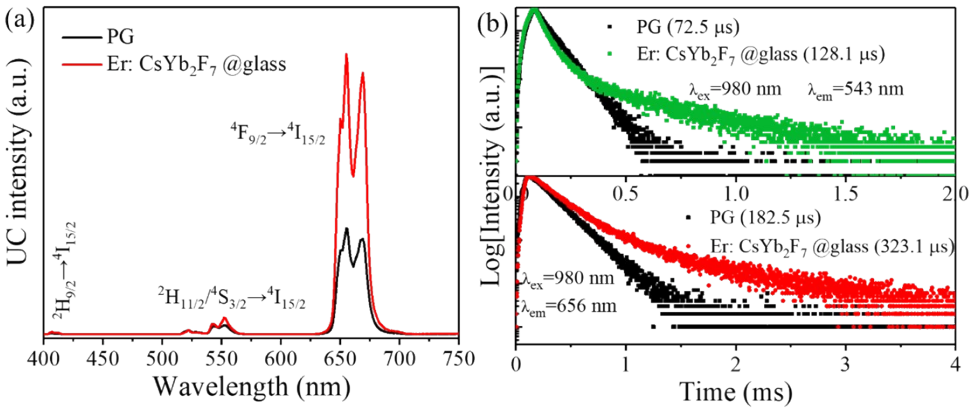

Fig. S4. (a) UC emission spectra of Er-doped PG and $CsYb_2F_7$ NCs@glass samples irradiated by 980 nm laser and (b) the corresponding decay curves by monitoring Er^{3+}: $^4S_{3/2} \rightarrow {}^4I_{15/2}$ (543 nm) and $^4F_{9/2} \rightarrow {}^4I_{15/2}$ (656 nm) transitions, respectively.

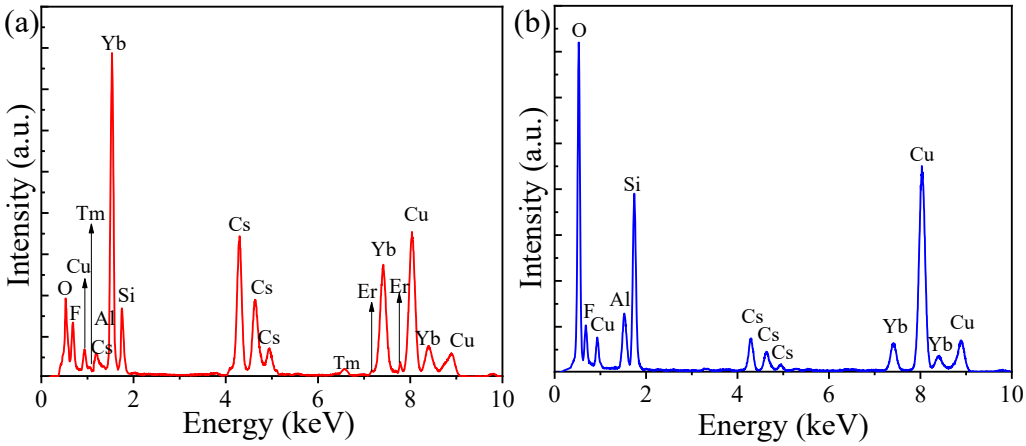

Fig. S5. EDX spectra from (a) an individual $CsYb_2F_7$ NC and (b) glass matrix in the Er/Tm co-doped $CsYb_2F_7$ NCs@glass composite. The Cu peaks are originated from the copper grid supporting the TEM sample.

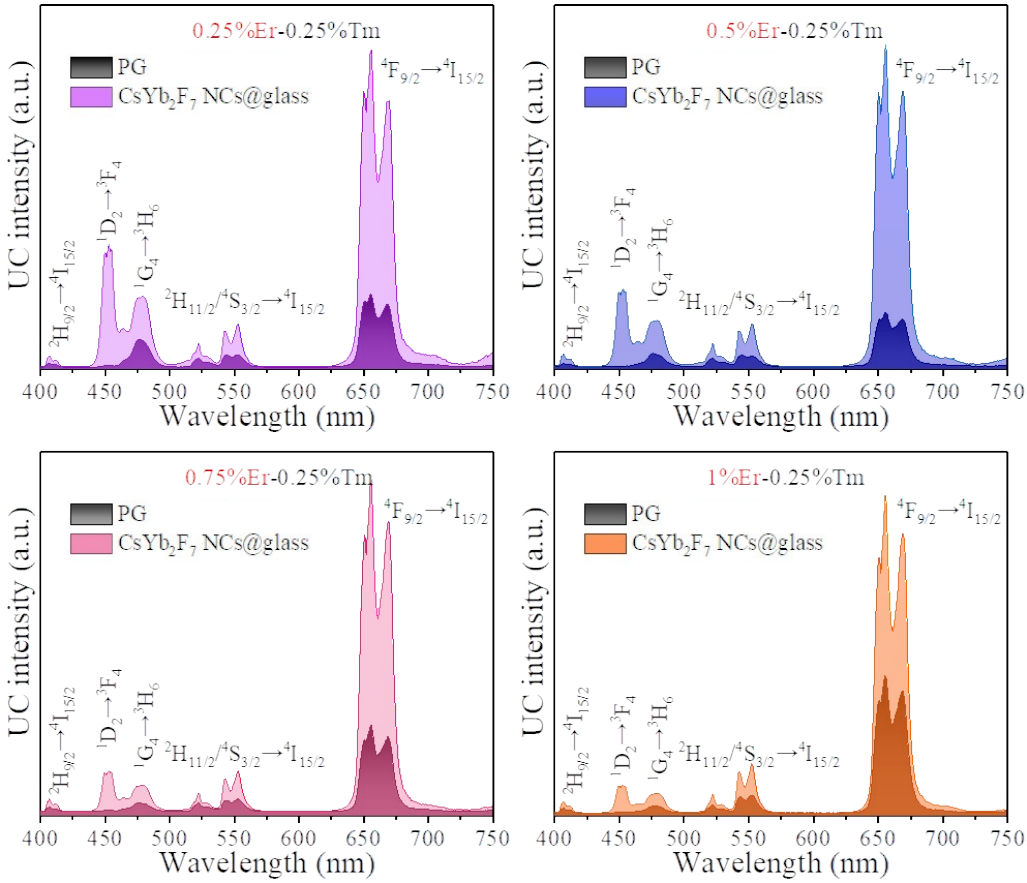

Fig. S6. UC emission spectra of Er/Tm co-doped PG and $CsYb_2F_7$ NCs@glass samples with various Er^{3+} contents and fixed Tm^{3+} content irradiated by 980 nm laser.

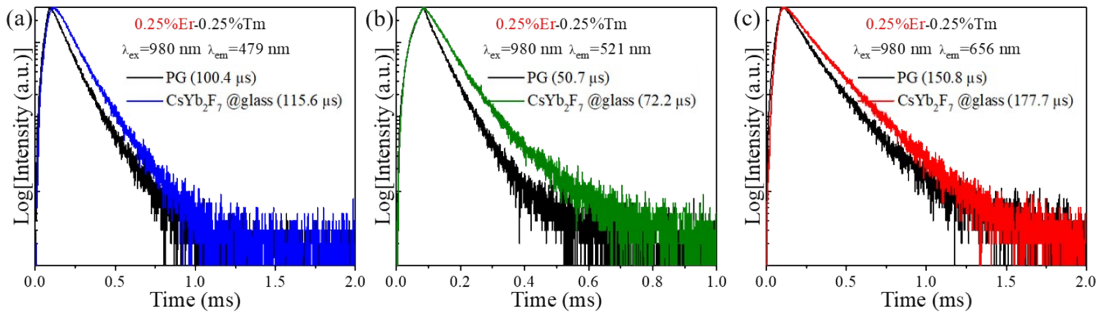

Fig. S7. UC decay curves of Er/Tm co-doped PG and $CsYb_2F_7$ NCs@glass by monitoring (a) Tm^{3+}: $^1G_4 \rightarrow {}^3H_6$ (479 nm), (b) Er^{3+}: $^2H_{11/2}, {}^4S_{3/2} \rightarrow {}^4I_{15/2}$ (521 nm), and (c) Er^{3+}: $^4F_{9/2} \rightarrow {}^4I_{15/2}$ (656 nm) transitions, respectively.

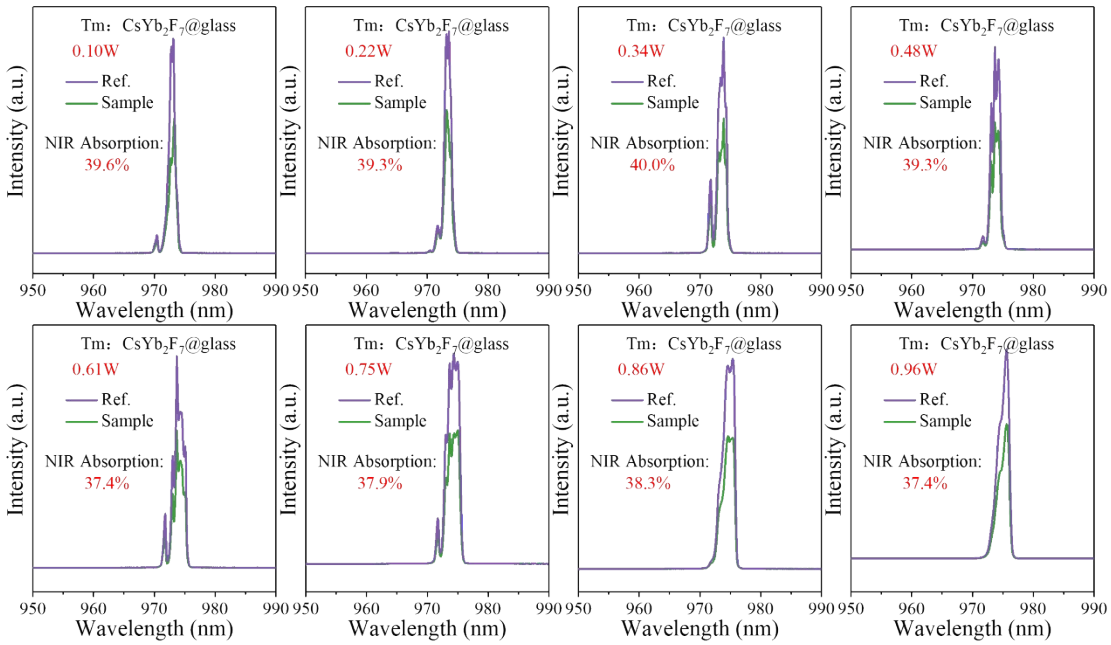

Fig. S8. Quantitative scattering spectra of Tm: $CsYb_2F_7$ NCs@glass and the reference for absolute absorption measurement of 980 nm laser with different laser powers.

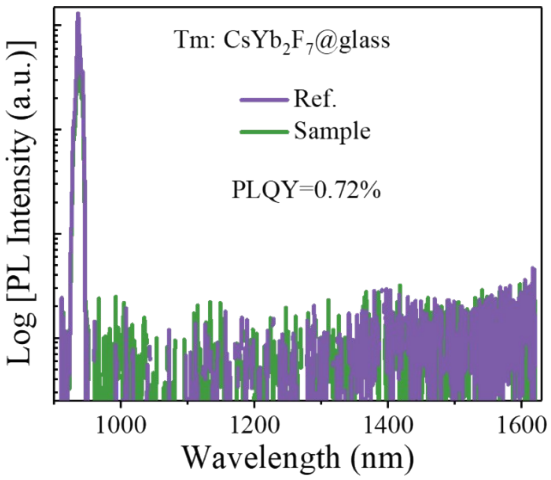

Fig. S9. Quantitative NIR PL spectra of Tm: $CsYb_2F_7$ NCs@glass and the reference for absolute PLQY determination.

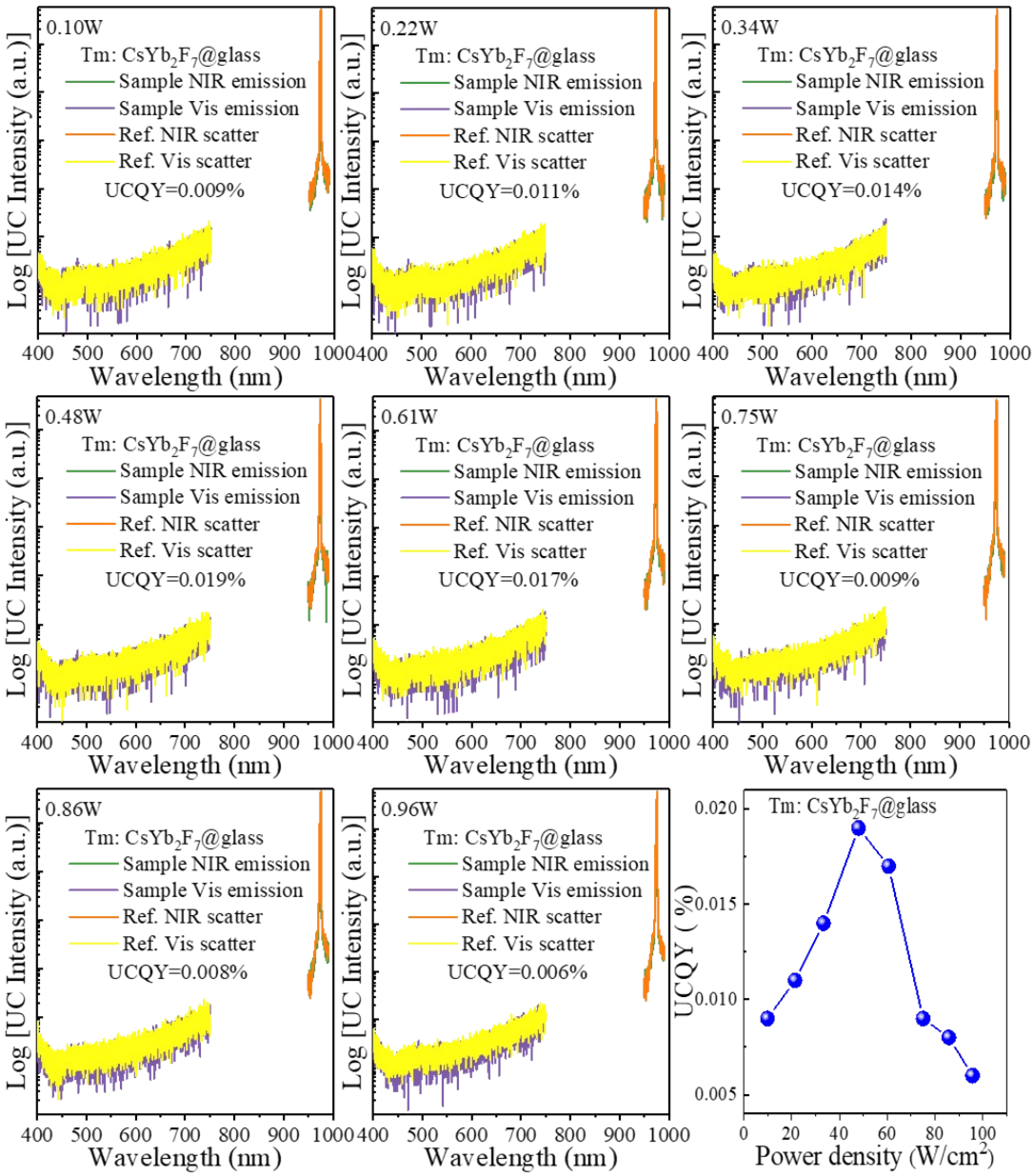

Fig. S10. Quantitative UC emission spectra of Tm: $CsYb_2F_7$ NCs@glass and the reference for UCQY determination by using different laser powers.

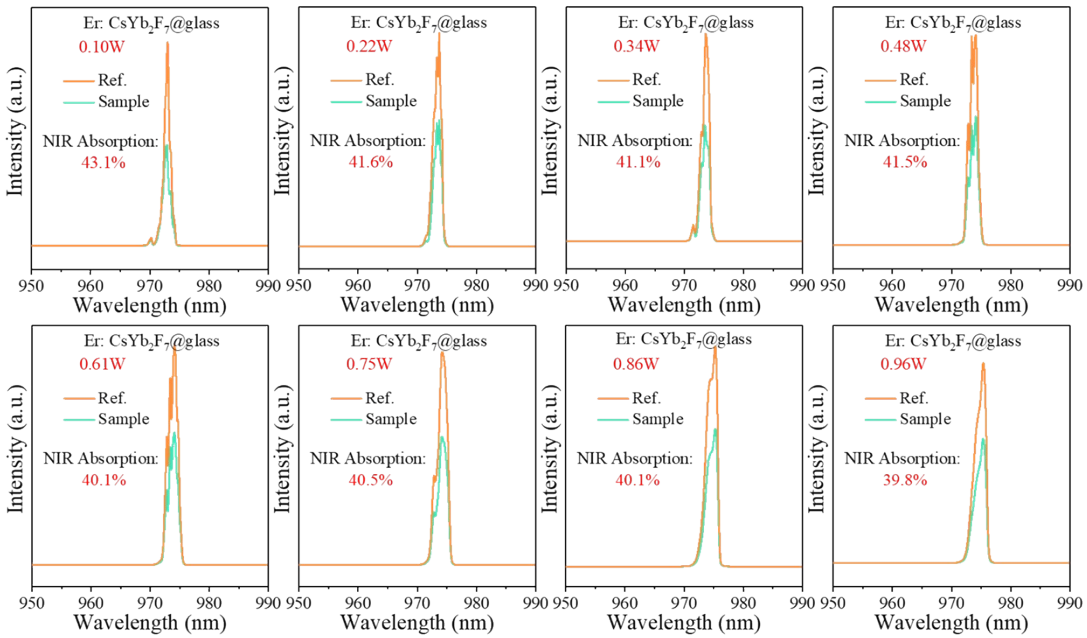

Fig. S11. Quantitative scattering spectra of Er: $CsYb_2F_7$@glass and the reference for absolute absorption measurement of 980 nm laser with various laser powers.

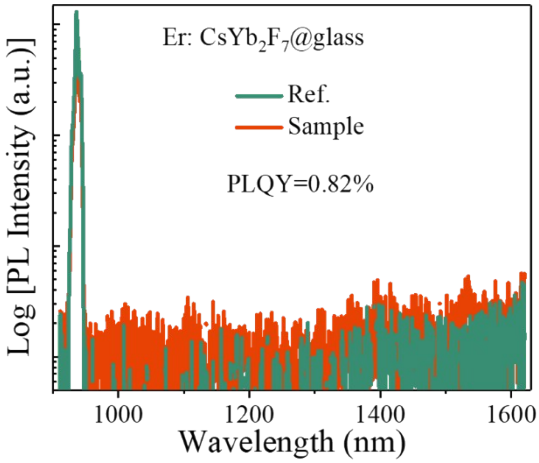

Fig. S12. Quantitative NIR PL spectra of Er: $CsYb_2F_7$ NCs@glass and the reference for absolute PLQY determination.

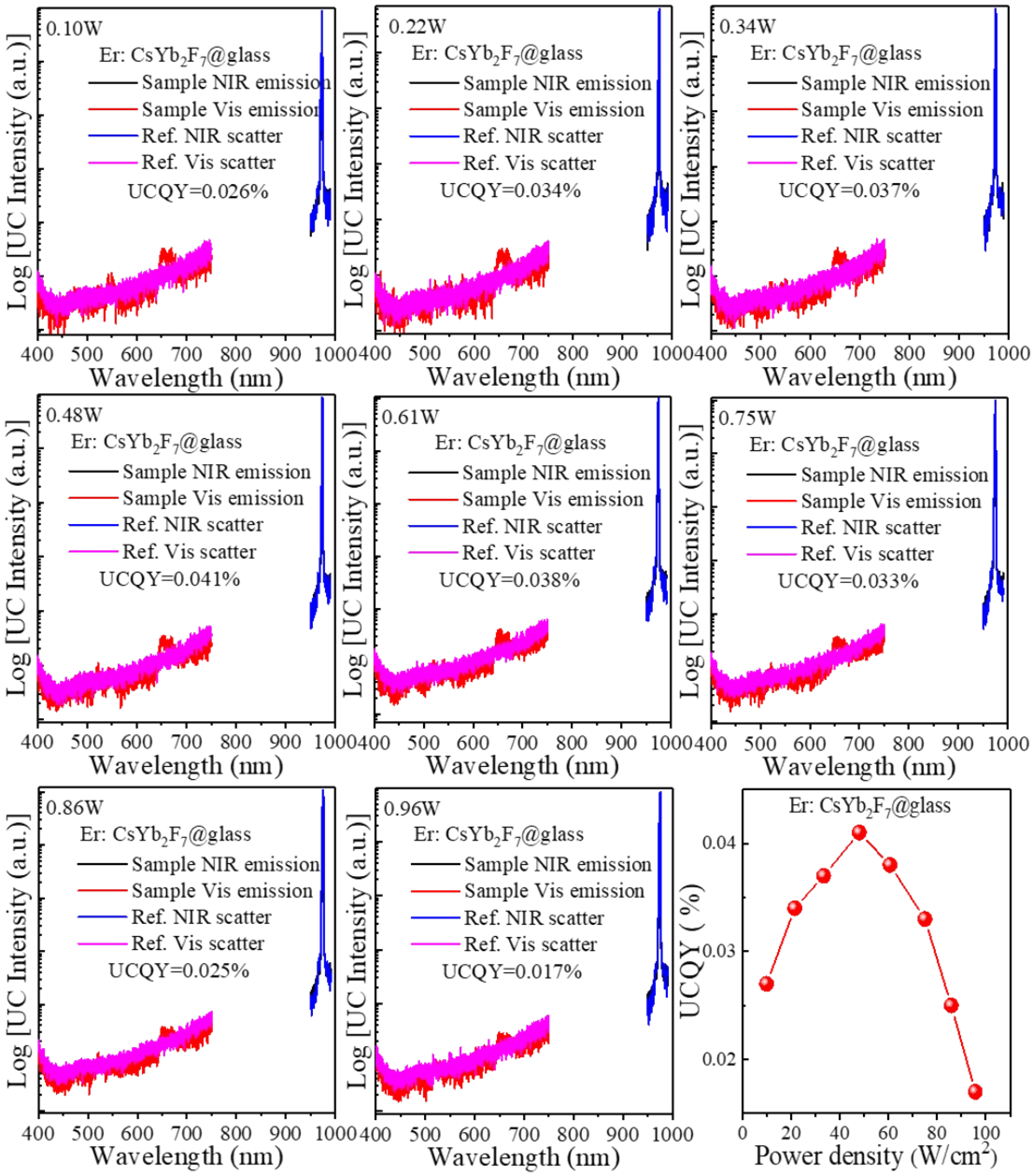

Fig. S13. Quantitative UC emission spectra of Er: $CsYb_2F_7$ NCs@glass and the reference for UCQY determination by using different laser powers.

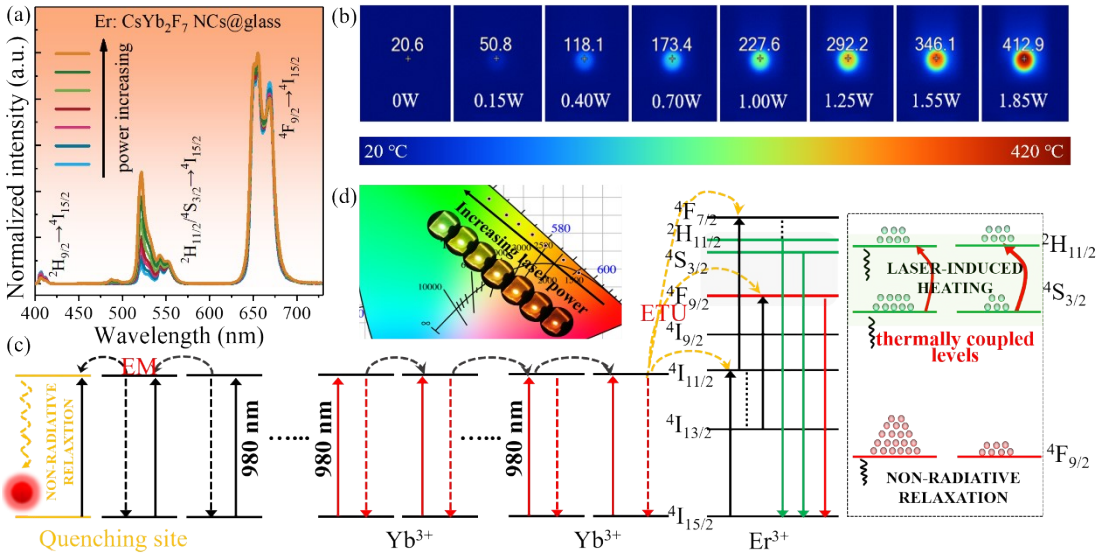

Fig. S14. (a) Laser power dependent UC emission spectra of Er: $CsYb_2F_7$ NCs@glass sample. All the spectra are normalized to Er^{3+}: 656 nm red emissions. (b) Alteration of the actual temperature for the Er: $CsYb_2F_7$ NCs@glass sample with the increase of laser power. (c) Schematic illustration of energy transfer processes between Yb-Er couples, ETU and EM represent energy transfer UC and energy migration, respectively. (d) Laser power dependent CIE color coordinates and the corresponding UC luminescence photographs of Er: $CsYb_2F_7$ NCs@glass.

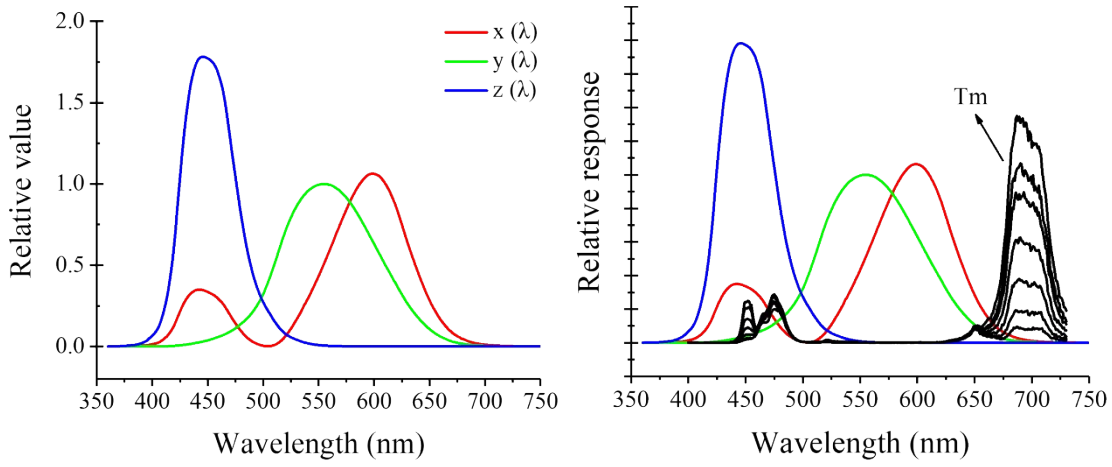

Fig. S15. The spectral response of tristimulus values and their response to Tm^{3+} emissions.

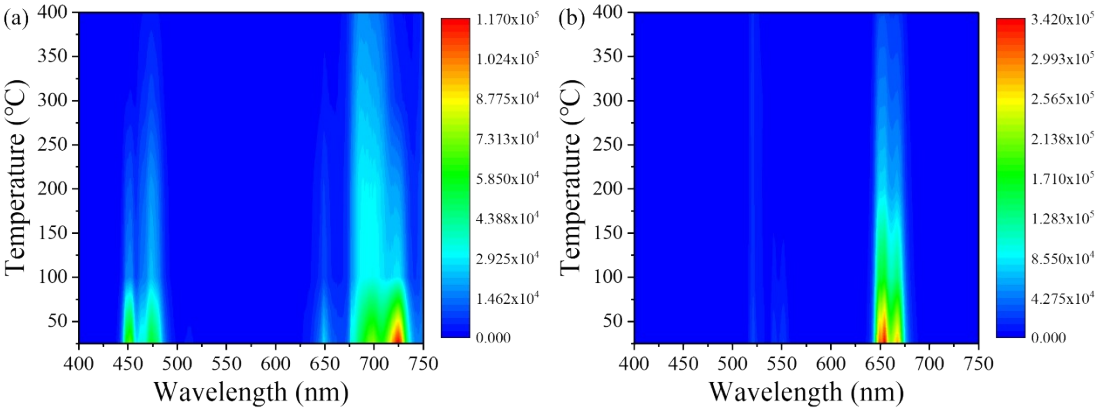

Fig. S16. Temperature dependent contour mappings of UC spectra for (a) Tm and (b) Er: $CsYb_2F_7$ NCs@glass samples (λ_{ex}= 980 nm).

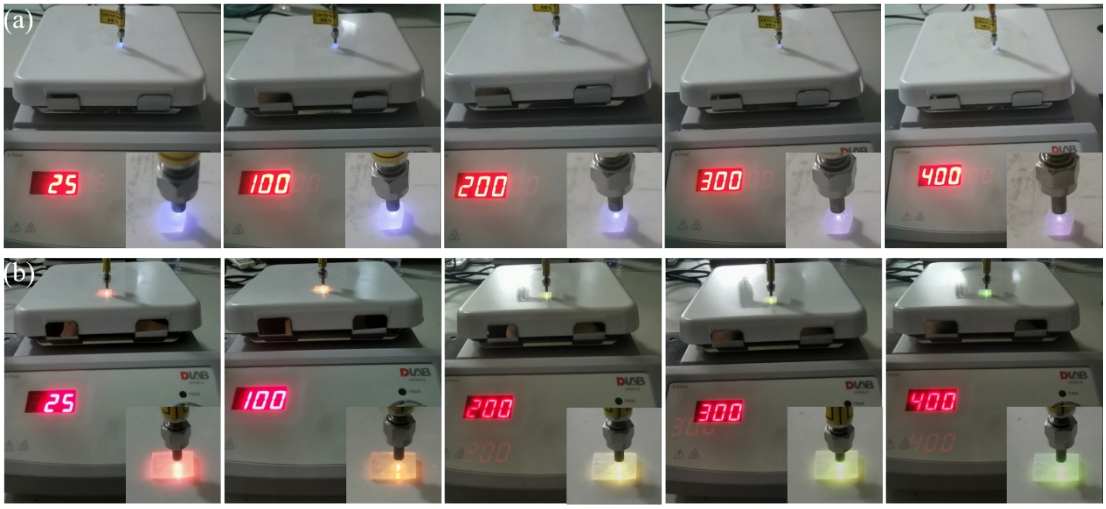

Fig. S17. Real-time observation of the change of UC emitting color for (a) Tm: and (b) Er: $CsYb_2F_7$ NCs@glass on a hot plate with elevation of temperature from 25 ℃ to 400 ℃ under NIR laser irradiation with a fixed power of 0.4 W.

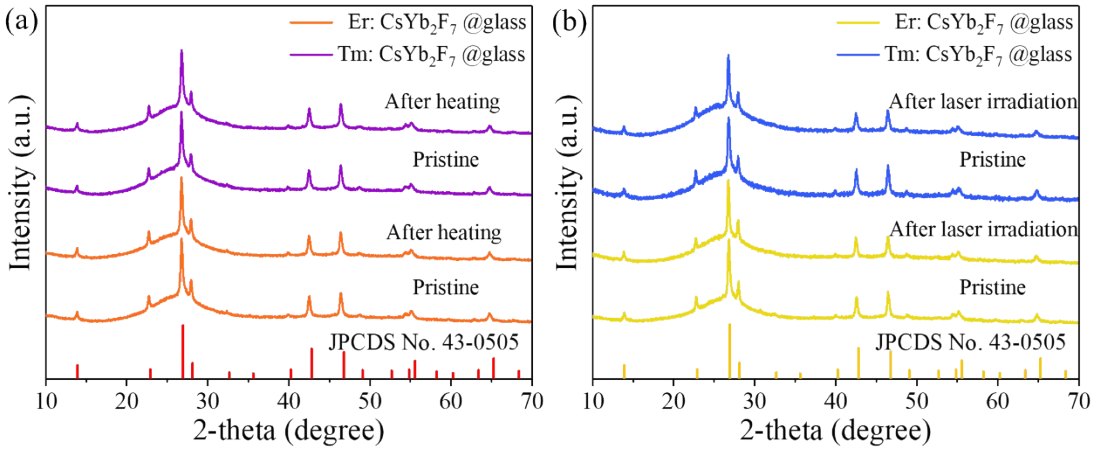

Fig. S18. XRD patterns of Tm and Er single-doped $CsYb_2F_7$ NCs@glass. (a) Before and after heating on a hot plate at 400 ℃ for 1 hour and (b) before and after 980 nm laser irradiation (1.85 W) for 30 min.

When irradiated by a 980 nm laser, the focal temperature of the sample rises rapidly through continuous heat accumulation, and reaches heat balance within 2 min. Therefore, after up to 30 min of laser irradiation (1.85 W), the temperature of the sample (~400 °C) has reached heat balance.

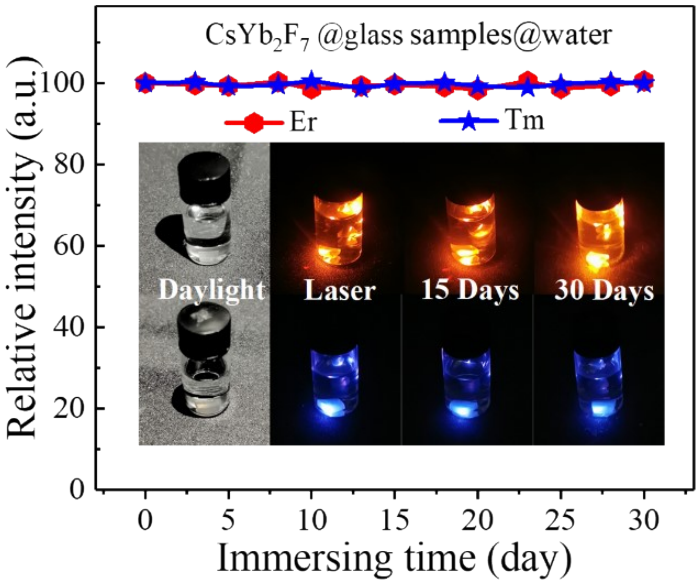

Fig. S19. The stability test of Tm-doped and Er-doped $CsYb_2F_7$ NCs@glass samples by directly immersing them in water, showing that the UC intensities remain unchanged after storing in water for 30 days.

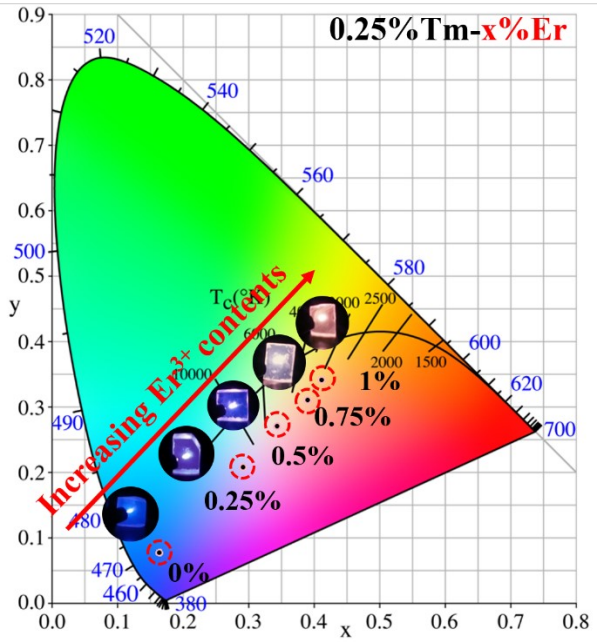

Fig. S20. Dependence of CIE color coordinates for a series of Er/Tm (x/0.25, mol%): $CsYb_2F_7$ NCs@glass samples with different Er^{3+} doping contents (x=0, 0.25, 0.50, 0.75, 1.00).

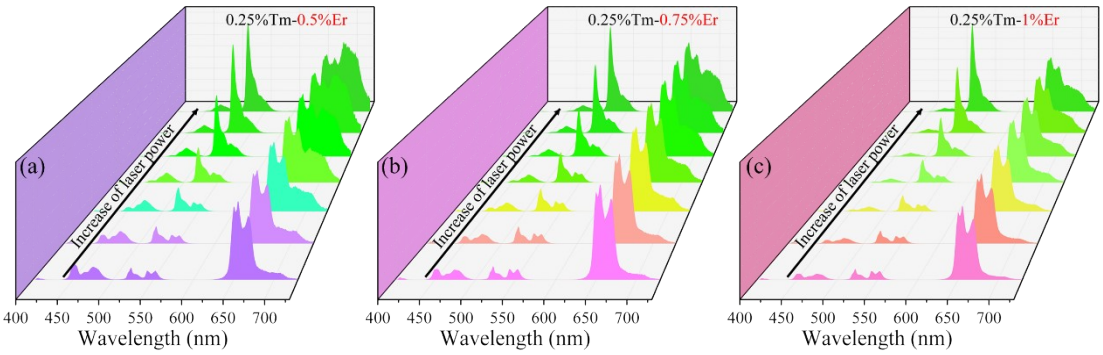

Fig. S21. Laser power dependent UC emission spectra for the Er/Tm (x/0.25, mol%): $CsYb_2F_7$ NCs@glass samples, (a) x=0.5, (b) x=0.75 and (c) x=1. All the spectra are normalized to Er^{3+} 656 nm red emission.

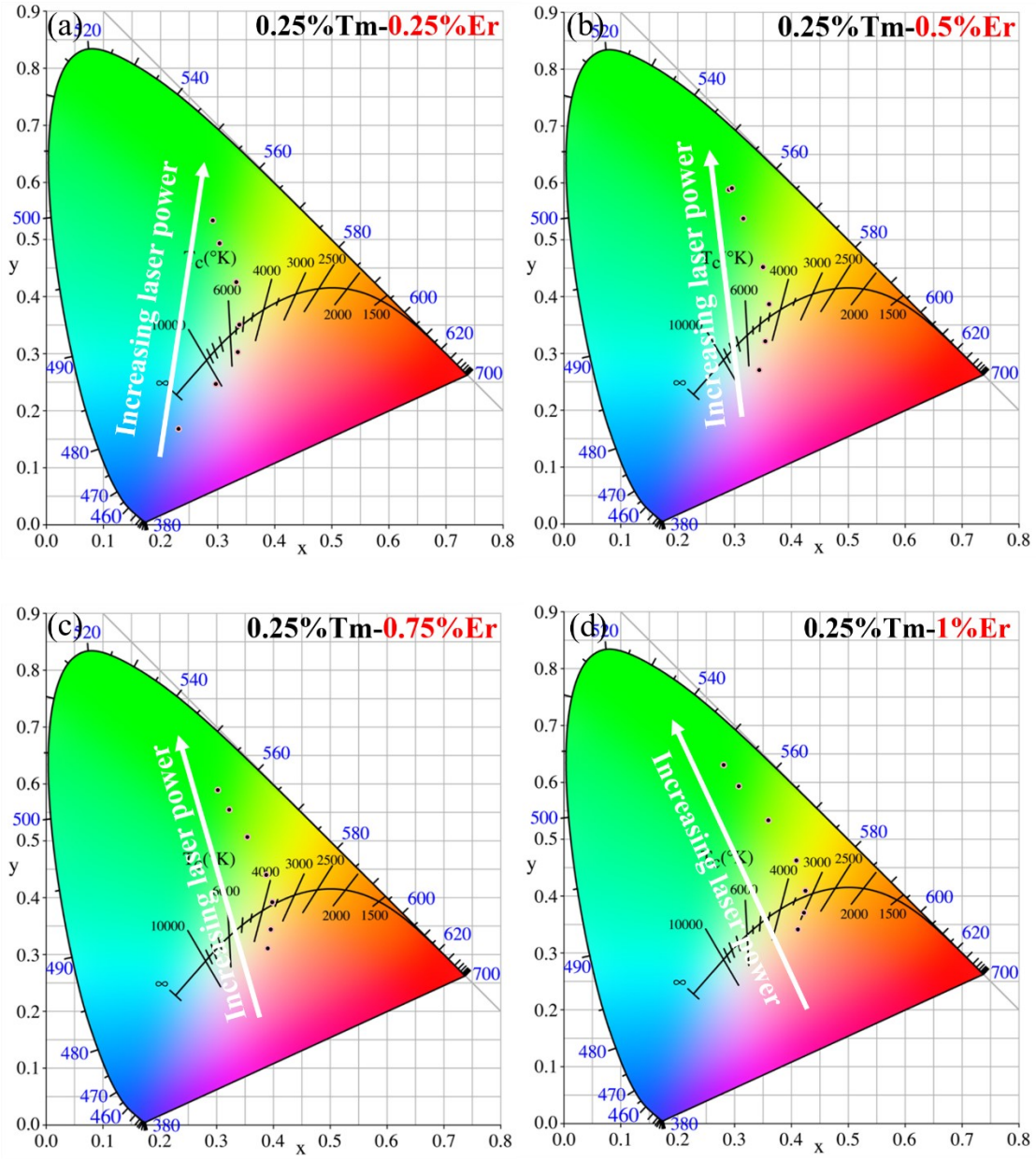

Fig. S22. Laser power dependent CIE color coordinates for the Er/Tm (x/0.25, mol%): $CsYb_2F_7$ NCs@glass samples, (a) x=0.25, (b) x=0.5, (c) x=0.75 and (d) x=1.

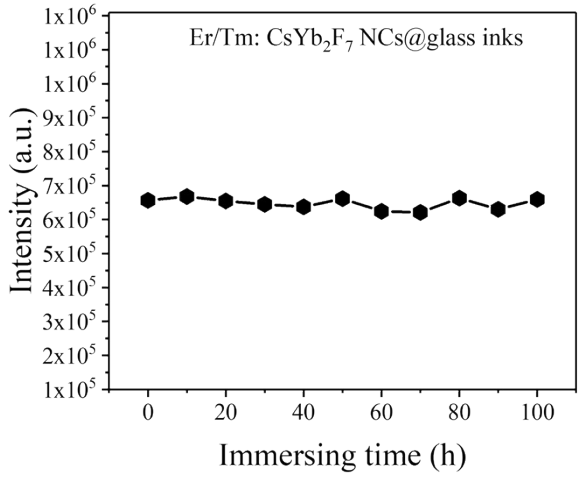

Fig. S23. The stability tests on anticounterfeiting patterns by immersing the patters in water for a certain time, showing almost unchanged of the UC intensity after immersing in water for 100 h.